Composites

CrossMark

Analyzing the frequency and temperature dependences of the ac conductivity and dielectric analysis of reduced graphene oxide/epoxy polymer nanocomposites

Y. Nioua[1] , S. El Bouazzaoui[1] , B. M. G. Melo[2] , P. R. S. Prezas[2] , M. P. F. Graça[2] ,
M. E. Achour[1] , L. C. Costa[2] , and C. Brosseau[3,*]

[1] *LASTID, Department of Physics, Faculty of Sciences, University Ibn Tofail, BP 133, 14000 Kenitra, Morocco*
[2] *I3N and Physics Department, University of Aveiro, 3810-193 Aveiro, Portugal*
[3] *Lab-STICC, Université de Brest, CS 93837, 6 avenue Le Gorgeu, 29238 Brest Cedex 3, France*

ABSTRACT

A series of composite materials was fabricated by mixing reduced graphene oxide (rGO) powder particles in an epoxy resin. In this paper, we analyze impedance measurements on these materials over broad frequency and temperature ranges. The real and imaginary parts of the effective complex impedance are well fitted to the Cole–Cole equation. The frequency dependence of the ac conductivity follows Jonscher's law with relaxation processes characterized by a broad distribution of relaxation times. The imaginary part of the effective electric impedance collapses onto a single master curve using a single characteristic frequency as a scaling parameter. We find that the electrical properties of the samples are strongly influenced by graphene oxide content. Below percolation threshold, the ac transport can be interpreted as due to electron hopping. Further, we find that the frequency-dependent effective impedance measurements overlap on a single master curve in the range of temperatures explored, showing that a single electrical conduction mechanism is operative. Close and above percolation threshold, the ac conduction originates from both electron tunneling and capacitive paths among the rGO nanoparticles in the polymer bulk.

Introduction and background

In the last decade, there has been experimental evidence of significantly modified electromagnetic properties of graphene (GE)-filled polymer nanocomposites which can be explored as a potential approach to engineering the microwave absorption and electrical properties of multifunctional materials [1–21]. The needs of today advanced multifunctional materials have moved well beyond the requirements of the effective medium and percolation analysis and now are focused on such concerns as 3D printing,

Address correspondence to E-mail: brosseau@univ-brest.fr

nano-ink, bioinspired and biocompatible structures and flexible substrate electronics.

Currently, the relevant length scales for the development of electronic devices are of the orders of a few tens of nanometers. GE nanosheet produced by mechanical exfoliation, with its exceptional strength, flexibility, electronic properties and chemical stability, is the ultimate soft but strong two-dimensional material. It provides an intuitive basis for nanocomposites with exceptional properties. With the advent of flexible electronics, GE-filled polymers are a rich setting for the study of multifunctional nanostructures. In parallel with this new work on soft nanocomposites, there has been an explosion of interest in the electric field control of the polarization in ferroelectric materials [22, 23], e.g., use of ferroelectricity to control the charge carriers in the graphene network. From an applications perspective, these ferroelectric nanomaterials can be used in voltage tunable devices such as MEMS, phase shifters [24], ferroelectric/GE FET nonvolatile memory device [25–27], electronic skin [28], energy harvesters and flexible actuators [29–31]. In order for these devices to function efficiently, the tunability versus temperature, electric field, mechanical stress and graphene content needs to be precisely controlled.

The work in Refs. [32, 33] has analyzed the dc electrical transport in reduced graphene oxide (rGO) powder particles dispersions in an epoxy resin (diglycidyl ether of bisphenol A) from 240 to 400 K. For this purpose, rGO-filled polymer samples prepared with different rGO content and thickness were fabricated. The focus in Refs. [32, 33] was on the dc electrical conductivity increases with increasing the rGO content and temperature. It is important to take note that there is a negative temperature coefficient in resistivity (NTCR) for rGO concentrations below the percolation threshold ϕ_{2c} ($\phi_{2c} \approx 4$ vol% [32, 33]), while a positive temperature coefficient in resistivity (PTCR) effect is observed above the percolation threshold. Significant challenges exist in investigation of multifunctional graphene oxide-filled polymer composites, e.g., tailoring the TCR for sensing applications.

This paper reports on impedance measurements of the percolative samples described in Refs. [32, 33] and makes connection with the charge transport under alternating field and temperature variations. Within the frequency range 10^2–10^6 Hz, impedance analysis is usually used to study relaxation processes,

i.e., polarization and conduction, in soft materials as function of temperature and frequency [34–37]. Such analyzers evaluate the effective impedance $Z^* = Z' - jZ'' = R_s - (2\pi j F C_s)^{-1}$ of a circuit in which the sample is inserted into a parallel plate capacitor. In the above, Z' and Z'' are, respectively, the real and imaginary parts of impedance, $F = \omega/2\pi$ is the frequency of the ac field and $\varepsilon_0 \approx 8.85 \times 10^{-12}$ Fm^{-1}. If C_0 is the geometrical capacitance of the sample (without sample), then $\varepsilon' = C_s/C$ and $\varepsilon'' = 1/2\pi R_s C_0 F$. From the measurement of Z^*, the ac conductivity σ_{ac} is determined and can give information on the short-range charge hopping rate of carriers which is complementary to the long-range dc conductivity. From the microstructural standpoint, when a disordered material composed of a random distribution of conducting and insulating phases is subjected to an ac field, the dipoles orient in the direction of the applied field with a broad distribution of characteristic relaxation time τ.

Our primary interest here is to understand the ac impedance behavior of graphene oxide/epoxy polymer nanocomposites over a broad range of frequency. The focus of our paper is to examine the charge transport mechanism in these composite materials, i.e., charge hopping of mobile carriers, and illustrate how rGO content and temperature can influence the ac conductivity.

This paper is organized as follows. Section two considers materials and the electromagnetic measurement methods. This section provides a brief recap of the effective impedance measurement using the equivalent circuit model and analysis methods. Next, the experimental results are presented in section three. By varying temperature and frequency of the electromagnetic wave, we find a variety of behaviors of the ac transport mechanisms which nicely complement the dc characterization of the samples described in Refs. [32, 33]. Section four gives a summary and conclusions.
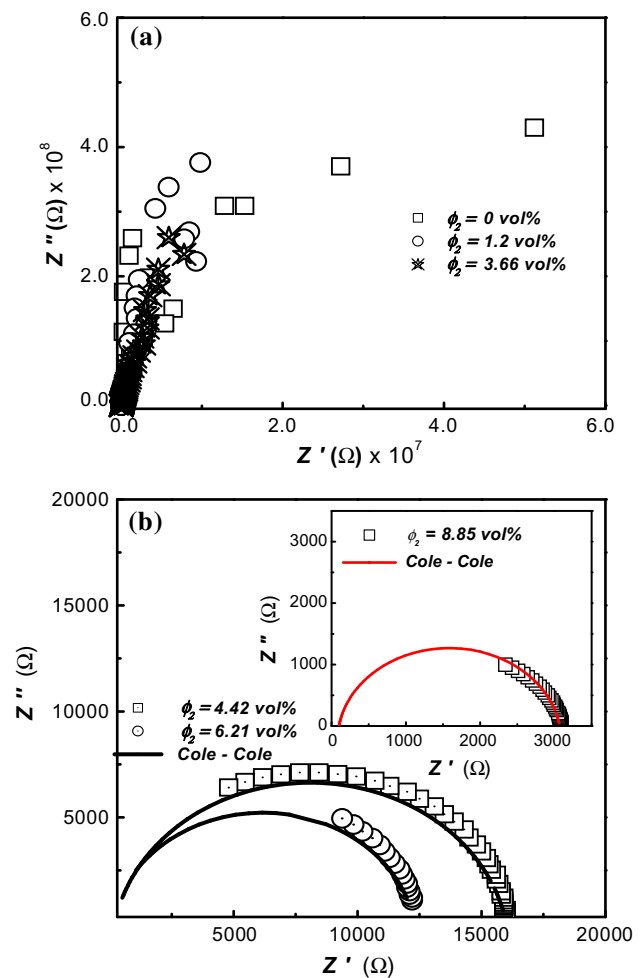
Experimental

Materials

The polymer phase is a commercially available liquid epoxy resin DER 321 obtained from Dow Chemicals Company. DER 321 is ortho-cresyl glycidyl ether diluted standard bisphenol A liquid-based epoxy
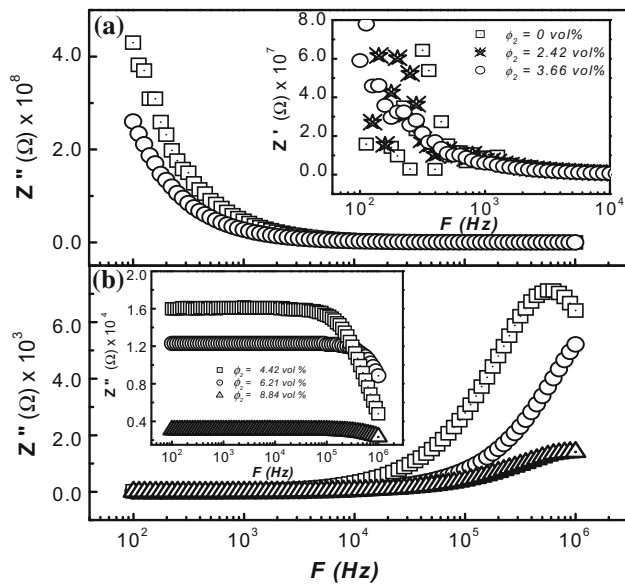
Figure 1 a The real and imaginary parts of the effective impedance of samples with rGO concentrations below the percolation threshold volume fraction $\phi_{2c} = 4$ vol%. $T = 300$ K; **b** as in (**a**) above the percolation threshold.

resin, of extremely low viscosity, e.g., 500–700 mPa s at 25 °C, epoxy equivalent weight 180–188 g/eq and density at 25 °C of 1.14 g ml^{-1}. The rGO particles powder is purchased from Graphenea Company (Gipuzkoa, Spain), with an average size of primary rGO particles about 260–295 nm, density of 1.91 g cm^{-3}, specific surface area of 423–500 m^2 g^{-1} and electrical conductivity of 667 S m^{-1} (measured in a 20-nm film thickness). The fabrication of the rGO-filled epoxy samples is realized using mechanical shear mixing through stirring. The mixing time was set to 24 h. In the first step, the desired volume fraction of rGO was mixed with the pre-polymer. This step was followed by samples curing for 24 h. The mixture of DER 321 and rGO particles was processed with an amine curing agent (4,9-dioxadodecan-1,12-diamine, equivalent weight = 81, supplied by BASF, and used without further purification). The ratio by weight of the mixture of the DER 321 and rGO particles to the amine curing agent was adjusted to achieve stoichiometry. Gelation took 5 min for each sample after pouring the mixture into the mold. Samples were unmolded after a few hours and left to rest after 24 h in order to complete polymerization. Eight series of specimens with 0 (pure resin), 2, 3, 4, 6, 8, 10 and 14 wt%, of rGO are fabricated. The samples

Figure 2 a Argand representation of the effective impedance of samples with rGO concentration below the percolation threshold volume concentration. Room temperature; **b** as in (**a**) above the percolation threshold. The *symbols* are the experimental data, and the *lines* are fits to CC equation.

consist of thick disks with nominal 15–18 mm diameter and 1.5–2 mm thickness. The glass transition temperature of the neat polymer is $T_g \approx 356$ K.

Impedance measurement method

Impedance spectroscopy measurements are taken in the temperature range 240–400 K with 5 K step in a continuous-flow He cryostat and in the frequency range of 100 Hz–1 MHz using an Agilent 4294A precision impedance analyzer operating in the C_s–R_s configuration. The response of the sample can be regarded as an equivalent circuit with a capacitance in parallel with resistance in the measurement.
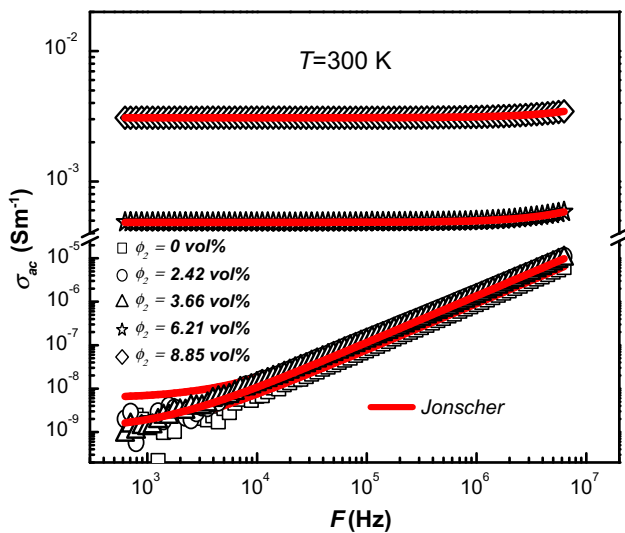
Results and discussion

Figure 1a reports the variation of the real and imaginary parts of Z* as a function of frequency for concentration below the percolation threshold at room temperature. Figure 1 shows the data that serve to make two points. Firstly, although insufficiently visible in Fig. 1a, the low-frequency behavior of Z″ is characterized by a single peak whose magnitude decreases as rGO volume fraction is increased. Secondly, the peak red shifts with increasing rGO volume fraction. The corresponding data for concentration above the percolation threshold are shown in Fig. 1b. The high-frequency peak is characterized by a single peak that blue shifts when rGO

Table 1 Dielectric relaxation parameters obtained by fitting the Z* data with Cole–Cole equation at different rGO concentrations above the percolation threshold

ϕ_2 (vol%)	τ (10^{-7} s)	ΔZ (kΩ)	α
4.42	0.98	15.80	0.11
6.21	2.7	12.23	0.10
8.85	4.7	3.39	0.11

$\Delta Z = Z_s - Z_\infty$. $T = 300$ K

volume fraction is increased. An Argand plane plot representation of the Z* data can be useful (Fig. 2) to provide information on the dielectric relaxation processes taking place in the sample. For single relaxation time Debye mechanism, a semicircular plot with center located in the Z′-axis is expected. However, when there is a distribution of the hopping rates in a disordered material, the Cole–Cole (CC) equation can be used, i.e., $Z^* = Z' - jZ'' = Z_\infty + \frac{Z_s - Z_\infty}{1 + (i\omega\tau)^{1-\alpha}}$, where Z_s and Z_∞ denote the values of impedance at low and high frequencies, respectively, and α is a

Table 2 Experimental values of n extracted from σ_{ac} using Jonscher's UPL

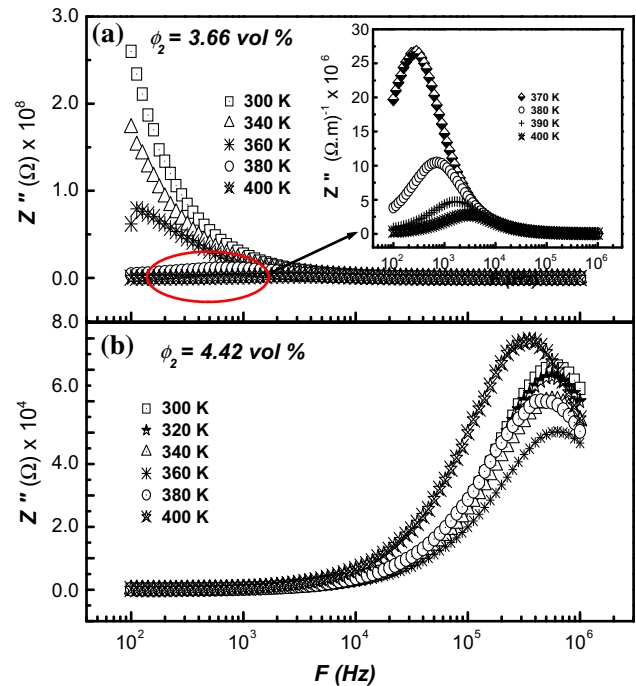| ϕ_2 (vol%)	σ_{dc} (Ω^{-1} m^{-1})	n	A
0	9.18×10^{-10}	1.05 ± 0.05	5.01×10^{-13}
2.42	5.97×10^{-9}	1.01 ± 0.02	1.25×10^{-12}
3.66	1.14×10^{-9}	1.00 ± 0.02	1.30×10^{-12}
4.22	4.8×10^{-4}	0.12 ± 0.03	9.8×10^{-5}
6.21	7.6×10^{-4}	0.03 ± 0.01	4.8×10^{-4}
8.85	3.0×10^{-3}	0.06 ± 0.03	1.07×10^{-3}

$T = 300$ K

Figure 3 The ac conductivity as a function of frequency for various rGO concentrations. Room temperature. Two regions can be seen: a plateau region and a frequency-dependent region which can be described by $\sigma_{ac} = \sigma_{dc} + A\omega^n$, where σ_{dc} is the dc conductivity, n is a frequency-independent exponent characterizing the subpercolative regime and A is a pre-exponential constant. The *red solid curve* represents a best fit to Jonscher universal power law.

Figure 4 **a** The imaginary part Z″ of the complex impedance as a function of frequency for different temperature values. $\phi_2 = 3.66$ vol%. The *inset* is a zoom of the region marked in *red*; **b** as in (**a**) for $\phi_2 = 4.42$ vol%.
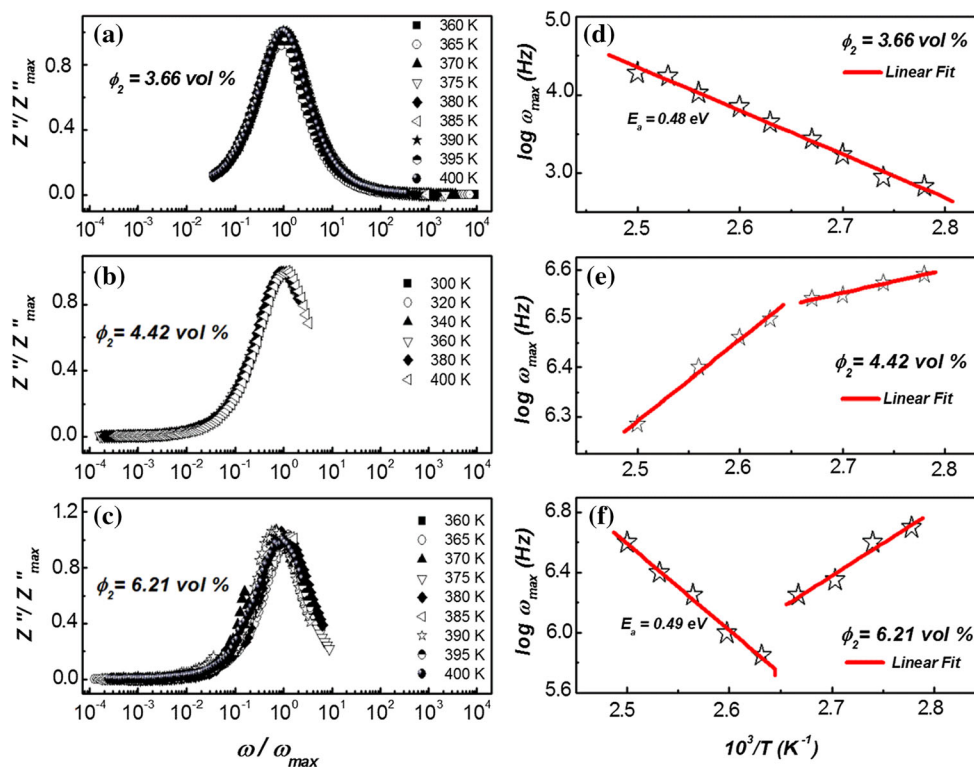
Figure 5 **a** Master imaginary part of the effective impedance curves for sample with $\phi_2 = 3.66$ vol%. The imaginary part of the impedance spectra data collapses into a single master curve $Z''/Z_{max} = f(\omega/\omega_{max})$ where f is a temperature-independent scaling function; **b** as in (**a**) for sample with $\phi_2 = 4.42$ vol%; **c** as in (**a**) for sample with $\phi_2 = 6.21$ vol%; **d** ω_{max} as a function of T^{-1} for sample with $\phi_2 = 3.66$ vol%. The *red line* connects the data points; **e** as in (**d**) for sample with $\phi_2 = 4.42$ vol%. When T approaches ≈ 373 K, a significant change in slope can be observed; **f** as in (**d**) for sample with $\phi_2 = 6.21$ vol%.

measure of the relaxation time distribution. Here, we find that $\alpha \approx 0.11$ for samples with rGO volume fraction ranging from 4.42 to 8.85 vol% (Table 1). Thus, for these supercolative samples, the relaxation is non-Debye type and is consistent with a model of dielectric heterostructure with hopping among free-energy barriers with a broad distribution of relaxation times [34].

Figure 3 reports the room-temperature variation of σ_{ac} as a function of frequency for samples below and above the percolation threshold. We observe that σ_{ac} increases with frequency for rGO volume fraction less than percolation threshold and is almost constant at a value depending on the rGO volume fraction above the percolation threshold. The latter is reminiscent to the dc conductivity. The frequency dependence of σ_{ac} is well fitted (solid line in Fig. 3) to the conductivity–frequency dependence, as proposed by Jonscher and known as the universal power law (UPL) [34], $\sigma_{ac} = \sigma_{dc} + A\omega^n$, where σ_{dc} is the dc

conductivity (measured in Refs. [32, 33]), n is a frequency-independent exponent characterizing the subpercolative regime and A is a pre-exponential constant. Both A and n are temperature dependent. The fitting parameters A and n are summarized in Table 2. The $n \leq 1$ values are observed to decrease from $\cong 1$ to $\cong 0$ with increasing rGo content. This is consistent with the case of heterostructures filled consisting of random distributions of conducting nanoparticles in a dielectric phase [38, 39] since the n value can be related to the fraction of capacitive paths which are involved in the ac transport mechanism.
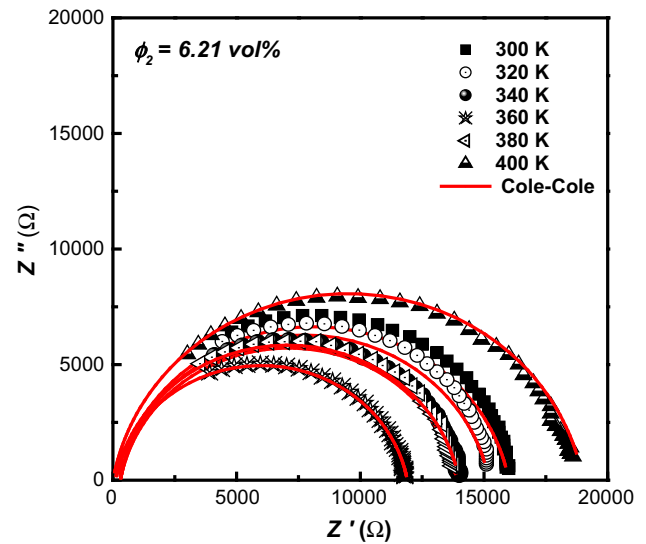
Figure 4 shows the plots of the variation of the Z^* data with frequency at various temperatures. Consider firstly sample below the percolation threshold ($\phi_2 = 3.66$ vol%). The dispersive regime is shifted toward high frequency when temperature is increased. This electron exchange interaction blurs electronic boundaries between non-interacting rGO
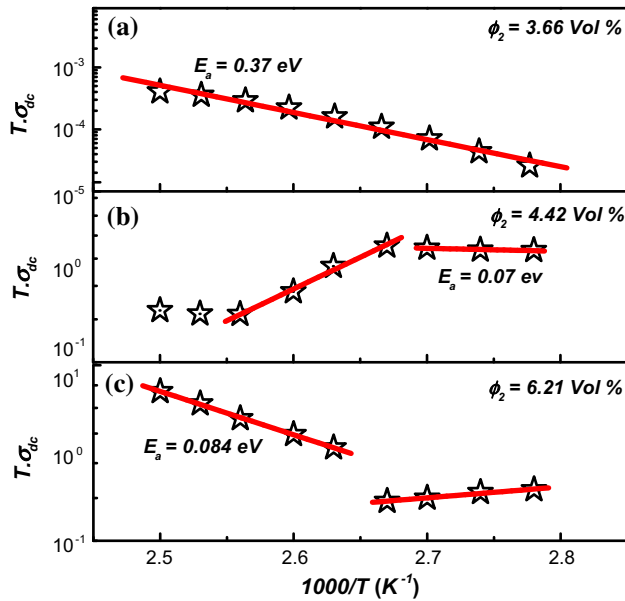
Figure 6 **a** $T\sigma_{dc}$ as a function of T^{-1} for sample with $\phi_2 = 3.66$ vol%. It is found that $T\sigma_{dc}$ is thermally activated with activation energy $E_{dc} = 0.37$ eV; **b** as in (**a**) for sample with $\phi_2 = 4.42$ vol%. When T approaches ≈ 373 K, a change in slope can be observed; **c** as in (**b**) for sample with $\phi_2 = 6.21$ vol%.

Figure 7 Argand representation for sample with rGO concentration above the percolation threshold volume fraction and different temperature values. The *red solid curve* represents a best fit to CC equation.

particles, resulting in blueshift of the Z'' peak. Above and close to percolation, an opposite redshift of the peak is observed. The bigger the number of electronically coupled rGO particles, the larger the redshift of the Z'' peak. Figure 5a shows the reduced master curve from plots of Z''/Z_{max} against ω/ω_{max} obtained at different temperatures for three rGO content values. This suggests that the transport mechanism in this range of temperature is characterized by a distribution of relaxation times which is temperature independent. Denoting by ω_{max} the frequency of the peak of Z'', it is found (Fig. 5d) that ω_{max} scales with $\exp\left(-\frac{E_{ac}}{kT}\right)$, where k is Boltzmann's constant. Below percolation threshold, the ac transport can be interpreted as due to electron hopping and charge carriers are thermally activated. The fitted value E_{ac} of 0.48 eV is close to established values of activation energy for similar polymer filled with carbonaceous inclusions [1–6, 17–19, 37, 38]. Next, we move to supercolative samples ($\phi_2 = 4.42$ vol% and $\phi_2 = 6.21$ vol%). Figure 5b shows the impedance master curve for several temperatures at $\phi_2 \approx \phi_{2c}$. The ω_{max} plot can no longer be accounted for by a single exponential but exhibits two different regions as function of T: (1) a monotonically increasing linear variation for $T > 377$ K ($T_g + 20$) and (2) a region

with different slopes for $T > 377$ K, which can be interpreted as a competition between tunneling and capacitive paths among rGO nanoparticles in the composite samples. In Fig. 5c corresponding to $\phi_2 > \phi_{2c}$, one sees a rapid decrease with slope $E_{ac} = 0.49$ for $T > 377$ K and slope change when one drops below 377 K. But in both cases, thermally activated tunneling conduction is evidenced. An increased hopping rate of charge carriers is observed with increasing T above ≈ 373 K. The comparison of the dc data shows that the change in slope in $\log(T\sigma_{dc})$ vs T^{-1} observed in Fig. 6b, c is close to that evidenced for $\log(\omega_{max})$ versus T^{-1} shown in Fig. 5. Hence, the ac conductivity is strongly correlated with the dc conductivity [32, 33] as shown in Fig. 6.

Figure 7 shows representative measurement results (Argand plots) of the effective impedance for sample with rGO volume fraction set to 4.42 vol% versus temperature. These data serve to make two important points. Firstly, the CC equation is valid for supercolative sample over the explored range of temperatures. This confirms that the dispersive non-Debye behavior is maintained in this range of temperature. Figure 8 shows the representative isotherms spectra of σ_{ac} for samples with $\phi_2 < \phi_{2c}$, $\phi_2 \approx \phi_{2c}$ and $\phi_2 > \phi_{2c}$, respectively. For each case, these isotherms clearly show a low-frequency plateau for a large portion of the spectrum and one sees a rapid increase at frequency higher than ≈ 0.1 MHz,
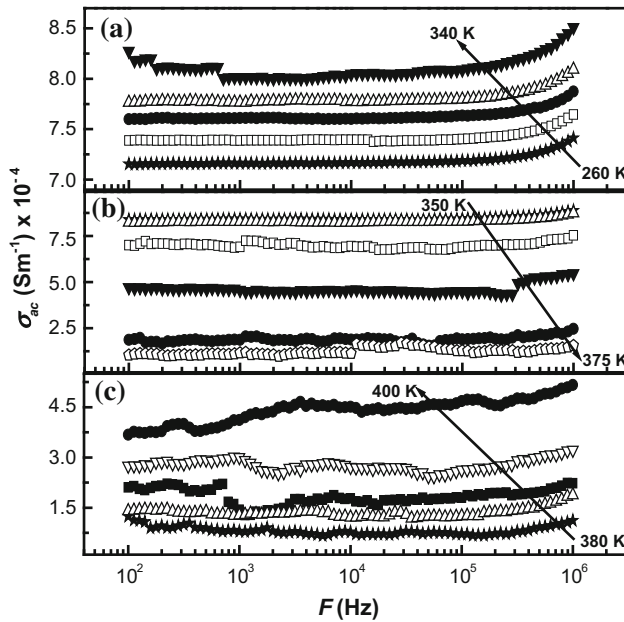
Figure 8 a Ac conductivity as a function of frequency for subpercolative sample with $\phi_2 = 3.66$ vol%. The *arrow* indicates the evolution of σ_{ac} as T is increased; **b** as in (**a**) for sample with $\phi_2 \approx \phi_{2c}$; **c** as in (**a**) above the percolation threshold.

i.e., hopping frequency. In the higher-frequency region, $\sigma_{ac}(\omega)$ increases due to the hopping of charge carrier in finite cluster. In order to analyze and understand the data presented above, it is necessary to consider three temperature ranges: temperature below 350 K (T_g) for which the conductivity increases with increasing temperature (Fig. 8a), which is typical for semiconducting material; as one moves to higher T from 350 to 380 K, the opposite behavior, typical for conducting material, is observed (Fig. 8b), and above 380 K (Fig. 8c), for which one sees the similar variation shown in Fig. 8a. Overall, one can say the temperature variation of σ_{ac} for this rGO polymer composite by adjusting the rGO loading is consistent with the PTCR effect [32, 33]. Furthermore, we would like to note that such information is critical for the development and optimization of the sensing capability of multifunctional polymer nanocomposites [39].

Concluding remarks

The above section has described measurement results on the electrical impedance and ac electrical conductivity of a composite material fabricated from

mechanical mixture. The dielectric processes taking place in the samples show trends consistent with a previous dc analysis [32, 33]. There are four main points of note for these experimental results: (1) the ac conduction shows a dispersive non-Debye behavior which can be described satisfactorily using CC equation over broad rGO content and temperature ranges; (2) the Jonscher's UPL is satisfied with an exponent value smaller than or close to one; thus, it is reasonable to expect that the relaxation processes are characterized by a broad distribution of relaxation times; (3) the imaginary part of the effective electric impedance collapses onto a single master curve using a single characteristic frequency as a scaling parameter which drives the relaxation processes; and (4) below percolation threshold, the ac transport can be interpreted as due to short-range electron hopping. Close and above percolation threshold, the ac conduction originates from both electron tunneling and capacitive paths among the rGO nanoparticles in the polymer bulk.

Compliance with ethical standards

Conflict of interest The authors declare that they have no conflict of interest.

References

[1] Adohi BJ-P, Byvhanok D, Haidar B, Brosseau C (2013) Microwave and mechanical properties of quartz/graphene-based polymer nanocomposites. Appl Phys Lett 102: 072903(1)–072903(5)

[2] Adohi BJ-P, Laur V, Haidar B, Brosseau C (2014) Measurement of the microwave effective permittivity in tensile-strained polyvinylidene difluoride trifluoroethylene filled with graphene. Appl Phys Lett 104:082902(1)–082902(5)

[3] Adohi BJ-P, Haidar B, Costa LC, Laur V, Brosseau C (2015) Assessing the role of graphene content in the electromagnetic response of graphene polymer nanocomposites. Eur Phys J B 88:280(1)–280(8)

[4] Adohi BJ-P, Brosseau C, Laur V, Haidar B (2017) Graphene controlled butterfly shape in permittivity-field loops of ferroelectric polymer nanocomposites. Appl Phys Lett 110:022902(1)–022902(5)

[5] Eletskii AV, Knizhnik AA, Potapkin BV, Kenny JM (2015) Electrical characteristics of carbon nanotube-doped composites. Phys Usp 58:209–251

[6] Bychanok D, Kuzhir P, Maksimenko S, Bellucci S, Brosseau C (2013) Characterizing epoxy composites filled with

carbonaceous nanoparticles from dc to microwave. J Appl Phys 113:124103(1)–124103(6)

[7] De Vivo B, Lamberti P, Tucci V, Guadagno L, Vertuccio L, Vittoria V, Sorrentino A (2012) Comparison of the physical properties of epoxy-based composites filled with different types of carbon nanotubes for aeronautic applications. Adv Polym Technol 31:205–218

[8] Khanam PN, Ponnamma D, Al-Madee MA (2015) Graphene-based polymer nanocomposites in electronics, Sadasivuni KK et al (eds). Springer, Berlin

[9] Marra F, D'Aloia AG, Tamburran A, Ochando IM, De Bellis G, Ellis G, Sarto MS (2016) Electromagnetic and dynamic mechanical properties of epoxy and vinylester-based composites filled with graphene nanoplatelets. Polymers 8:272(1)–272(18)

[10] Qin F, Brosseau C (2011) A review and analysis of microwave absorption in polymer composites filled with carbonaceous particles. J Appl Phys 111:061301(1)–061301(24)

[11] Zhao X, Zhang Z, Wang L, Xi K, Cao Q, Wang D, Yang Y, Du Y (2013) Excellent microwave absorption property of Graphene-coated Fe nanocomposites. Nat Sci Rep 3:3421(1)–3421(5)

[12] Sharifi T, Gracia-Espino E, Reza Barzegar H, Jia X, Nitze F, Hu G, Nordblad P, Tai C-W, Wågberg T (2013) Formation of nitrogen-doped graphene nanoscrolls by adsorption of magnetic γ-Fe_2O_3 nanoparticles. Nat Commun 4:2319(1)–2319(9)

[13] Bludov YV, Peres NMR, Vasilevskiy MI (2013) Unusual reflection of electromagnetic radiation from a stack of graphene layers at oblique incidence. J Opt 15:114004(1)–114004(7)

[14] Liu P, Huang Y, Zhang X (2014) Superparamagnetic $NiFe_2O_4$ particles on poly(3,4-ethylenedioxythiophene)–graphene: synthesis, characterization and their excellent microwave absorption properties. Compos Sci Technol 95:107–113

[15] Jang B, Zhamu A (2008) Processing of nanographene platelets (NGPs) and NGP nanocomposites: a review. J Mater Sci 43:5092–5101

[16] Yang Y, Rigdon W, Huang X, Li X (2013) Enhancing graphene reinforcing potential in composites by hydrogen passivation induced dispersion. Nat Sci Rep 3:2086(1)–2086(7)

[17] Kuilla T, Bhadra S, Yao D, Kim NH, Bose S, Lee JH (2010) Recent advances in graphene based polymer composites. Prog Polym Sci 35:1350–1375

[18] Potts JR, Dreyer DR, Bielawski CW, Ruoff RS (2011) Graphene-based polymer nanocomposites. Polymer 52:5–25

[19] Kim H, Abdala AA, Macosko CW (2010) Graphene/polymer nanocomposites. Macromolecules 43:6515–6530

[20] Stankovich S, Dikin DA, Dommett GHB, Kohlhaas KM, Zimney EJ, Stach EA, Piner RD, Nguyen ST, Ruoff RS (2006) Graphene-based composite materials. Nature 442:282–286

[21] Liang J, Wang Y, Huang Y, Ma Y, Liu Z, Cai J, Zhang C, Gao H, Chen Y (2009) Electromagnetic interference shielding of graphene/epoxy composites. Carbon 47:922–925

[22] Zhang ZC, Meng QJ, Chung TCM (2009) Energy storage study of ferroelectric poly(vinylidene fluoride-trifluoroethylenechlorotrifluoroethylene) terpolymers. Polymer 50:707–715

[23] Xia WM, Xu Z, Wen F, Li WJ, Zhang ZC (2010) Crystalline properties dependence of dielectric and energy storage properties of poly(vinylidene fluoride-chlorotrifluoroethylene). Appl Phys Lett 97:222905

[24] Tagantsev AK, Sherman VO, Astafiev KF, Venkatesh J, Setter N (2013) Ferroelectric materials for microwave tunable applications. J Electroceram 11:5–66

[25] Hu Z, Tian M, Nysten B, Jonas AM (2008) Regular arrays of highly ordered ferroelectric polymer nanostructures for nonvolatile low-voltage memories. Nat Mater 8:62–67

[26] Zheng Y, Ni GX, Toh CT, Tan CY, Yao K, Özyilmaz B (2010) Graphene field-effect transistors with ferroelectric gating. Phys Rev Lett 105:166602(1)–166602(5)

[27] Zheng Y, Ni GX, Toh CT, Zeng MG, Chen ST, Yao K, Özyilmaz B (2009) Gate-controlled nonvolatile graphene-ferroelectric memory. Appl Phys Lett 94:163505(1)–163505(5)

[28] Park J, Kim M, Lee Y, Lee HS, Ko H (2015) Fingertip skin-inspired microstructured ferroelectric skins discriminate static/dynamic pressure and temperature stimuli. Sci Adv 1:e1500661

[29] Bae S-H, Kahya O, Sharma BK, Kwon J, Cho HJ, Özyilmaz B, Ahn J-H (2013) Graphene-P(VDF-TrFE) multilayer film for flexible applications. ACS Nano 7:3130–3138

[30] Zhang S, Neese B, Ren K, Chu B, Zhang QM (2006) Microstructure and electromechanical responses in semicrystalline ferroelectric relaxor polymer blends. J Appl Phys 100:044113(1)–044113(6)

[31] Eda G, Franchini G, Chhowalla M (2008) Large-area ultrathin films of reduced graphene oxide as a transparent and flexible electronic material. Nat Nanotechnol 3:270–274

[32] Nioua Y, El Bouazzaoui S, Melo BMG, Prezas PRS, Achour ME, Graça MPF, Costa LC. Electrical studies on reduced graphene oxide/epoxy resin composites. J Comp Mater (in press)

[33] Boukheir S, Len A, Füzi J, Kenderesi V, Achour ME, Eber N, Costa LC, Oueriagli A, Outzourhit A (2016) Structural characterization and electrical properties of carbon

nanotubes/epoxy polymer composites. J Appl Polym Sci 134:44514(1)–44514(8)

[34] Jonscher AK (1977) The 'universal' dielectric response. Nature 267:673–679

[35] Almond DP, Bowen CR, Rees DAS (2006) Composite dielectrics and conductors: simulation, characterization and design. J Phys D Appl Phys 39:1295–1304

[36] Bowen CR, Almond DP (2006) Modelling the 'universal' dielectric response in heterogeneous materials using microstructural electrical networks. Mater Sci Technol 22:719–724

[37] Barsoukov E, Macdonald JR (2005) Impedance spectroscopy: theory, experiment and applications. Wiley Interscience, Hoboken

[38] Aribou N, EL Bouazzaoui S, Achour ME, Brosseau C (2014) Investigating the dielectric properties of carbon black-epoxy composites. Spectrosc Lett 47:336–340

[39] Gong S, Zhu ZH, Li Z (2017) Electron tunnelling and hopping effects on the temperature coefficient of resistance of carbon nanotube/polymer nanocomposites. Phys Chem Chem Phys 19:5113–5120